ES Energy & Environment

DOI: https://dx.doi.org/10.30919/esee8c1040

Sub-Picosecond Optical Response of Metals Due to Non-Thermalized Electron Dynamics

Long Li,[1,2] Liang Zhang,[1] Lenan Zhang,[3] Yang Zhong,[3] Evelyn N. Wang,[3] Zhen Chen[2,*] and Liang Guo[1,4,*]

Abstract

Non-thermalized electrons in metals, featured by deviation from the Fermi-Dirac distribution, have recently shown potential to facilitate realization of ultrafast photonic devices such as all-optical modulators. Dissection of non-thermalized electron dynamics and its influence on optical response of metals is therefore essential for optimization of photonic design. The sub-picosecond dynamics of non-thermalized electrons in gold, excited by femtosecond laser, is studied in this work combining electron Boltzmann transport equation and femtosecond spectroscopy. It is found that there are significant differences among the ultrafast reflectance signals detected with different probe photon energies in sub-picosecond timescale, which result from the evolution of non-thermalized electrons and cannot be described by temperature-based models. For the probe photon energy far away from the interband transition threshold (ITT) of gold, the transient reflectance signal is featured by short leading and tailing durations. While for the probe photon energy close to the ITT, the transient reflectance change exhibits much slower dynamics. By calculating the dynamics of the non-thermalized electron energy distribution, the origin of the ultrafast optical response is revealed. The analysis in this study could provide insights on electron-photon coupling to guide the design of ultrafast photonic devices based on metals.

Keywords: Sub-picosecond optical response; Non-thermalized electron; Femtosecond spectroscopy.
Received: 9 November 2020; Accepted: 19 December 2020.
Article type: Research article.

1. Introduction

In the past decades, micro/nanoscale heat conduction has drawn tremendous research interests.[1-3] In this field, non-classical heat transfer may occur, beyond the scope described by Fourier's law, and new frameworks are required to depict the rules of the unusual heat transport.[4] The microscopic non-equilibrium heat conduction, which is a typical non-classical thermal phenomenon, mainly includes three non-equilibrium heat transfer processes. First, electrons (or holes) and phonons may be out of equilibrium, with heat transfer occurring between the two systems. The duration of this process, depending on the electron-phonon (*e-ph*) coupling factor, ranges from 1 ps to 100 ps. The two-temperature model (TTM), which includes two coupled equations to describe the temperatures of electrons and phonons has shown excellent performance in modeling heat transfer when *e-ph* non-equilibrium is present.[5-7] Especially, the interfacial thermal transport is an important concern in micro/nanoscale heat transfer.[3,8-11] For example, the effective interfacial heat transfer in Au-Si system could be significantly enhanced by inserting a film with a larger *e-ph* coupling factor than that of Au.[12] When electrons and phonons were strongly out of equilibrium, the interfacial *e-ph* coupling could contribute to the thermal boundary conductance.[13] Additionally, phonons of different modes may also be in non-equilibrium. In this case, the phonon system cannot be described by the Bose-Einstein distribution and the phonon temperature becomes ill-defined. The duration of this state depends on the coupling strength among different phonon modes, which could be as long as 100 ps. Both calculated and experimental results show that non-equilibrium phonons must be considered in the measurement of thermal conductivity.[14,15] Finally, electrons (holes) in different states could also be out of equilibrium, characterized

[1] *Department of Mechanical and Energy Engineering, Southern University of Science and Technology, Shenzhen, China.*
[2] *Jiangsu Key Laboratory for Design & Manufacture or Micro/Nano Biomedical Instruments, School of Mechanical Engineering, Southeast University, Nanjing, China.*
[3] *Device Research Laboratory, Department of Mechanical Engineering, Massachusetts Institute of Technology, 77 Massachusetts Avenue, Cambridge, Massachusetts 02139, USA*
[4] *Key Laboratory of Energy Conversion and Storage Technologies (Southern University of Science and Technology), Ministry of Education, Shenzhen 518055, China.*
**Email:* zhenchen@seu.edu.cn (Z. Chen), guol3@sustech.edu.cn (L. Guo)

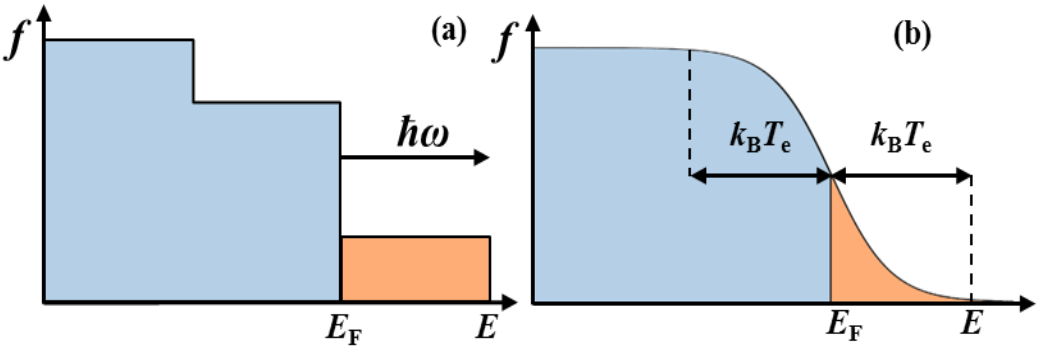

Fig. 1 Schematics of the electron energy distribution in (a) non-thermalized and (b) thermalized states. The blue and orange areas represent electron distribution below and above E_F, respectively.

by deviation from the Fermi-Dirac distribution, and the electron temperature becomes meaningless. Electrons in this state are called non-thermalized electrons, which is the focus of this study. For example, during the interaction between femtosecond laser and metals,[16, 17] electrons below the Fermi level E_F absorb the photon energy $\hbar\omega$ and undergo transitions to higher energy levels above E_F. Immediately after the interaction, the electron energy distribution severely deviates from the Fermi-Dirac distribution, as shown in Fig. 1 (a), and the electron system is non-thermalized. Due to electron-electron (*e-e*) scattering, the energy is rapidly exchanged among electrons. The electrons quickly become thermalized, and the energy distribution follows the Fermi-Dirac distribution, as shown in Fig. 1 (b) (k_B is the Boltzmann constant and T_e indicates the electron temperature). The relaxation time of non-thermalized electrons, which depends on the scattering strength among the electrons, is typically on the order of 10 to 100 fs.

Recently, taking advantage of the ultrafast transport properties of electrons, ultrafast optical modulation was realized based on metallic structures.[18-21] For example, based on ultrafast electron spatial transport induced by non-uniform electron temperature distribution, the optical switching time could be tuned from 200-500 fs.[21] In particular, the optical modulation based on ultrafast non-thermalized electrons dynamics has attracted much attention. For instance, by activating the interface relaxation pathway for non-thermalized electrons, femtosecond all-optical modulation of light amplitude was achieved based on gold nanostructure.[22] Ultrafast optical modulation of light phase and polarization was realized utilizing the ultrafast transport of non-thermalized electrons across the interface between a plasmonic metal layer and a charge acceptor.[23] Early works have been conducted about non-thermalized electron dynamics. The work of Sun *et al*. mentioned that the sub-picosecond optical responses of metals were deeply influenced by non-thermalized electron dynamics, but it mainly focused on the decay of the signal in picosecond timescale.[24] Comparing the optical responses of silver with gold, it was found that a weak *e-e* screening potential led to a short thermalization time of non-thermalized electrons and a fast decay of the signal.[25] Lisowski *et al*. found that in the femtosecond laser-Ru interaction, the existence of non-thermalized electrons not only had an important effect on the transient reflectance change in sub-picosecond but also reduced the heat transfer between electrons and phonons, but the numerical model cannot well reflect the non-thermalized electron dynamics on any energy level.[26] The non-thermalized electron dynamics in metals after femtosecond laser perturbation are theoretically studied by solving electron Boltzmann transport equation (BTE), considering the phonon energy distribution evolution, but the inducing optical response was not discussed.[27] A conversion model calculating the evolution of non-thermalized electrons from the transient reflectance was proposed by Gray *et al*., which provides a general method to get the non-thermalized electron dynamics from experimental data.[28] Despite these studies, attention has mostly been focused on the tailing part of the optical responses due to its importance to understand carrier relaxation. However, in terms of ultrafast photonics, the leading edge of the optical response, like the rising time of a photodetector, is equally important in determining the device performance, which has not yet been considered carefully.

In this work, the sub-picosecond optical response of metals including both the leading and the tailing edges is investigated by combining the electron BTE adopted to capture non-thermalized electron dynamics and femtosecond spectroscopy, which is performed to measure the ultrafast optical response. A fast decay of the transient reflectance was observed from the femtosecond spectroscopy when the probe photon energy is far away from the interband transition threshold (ITT). This transient reflectance cannot be well described by the conventional TTM, but can be well predicted by the electron BTE, which considered the contribution of non-thermalized electrons. Especially, calibration of the absolute time delay in femtosecond spectroscopy is performed in this work to unravel the timing relation between the optical responses by different probe photon energies. Therefore, the relationship between the sub-picosecond optical response and the dynamics of electrons is revealed, which provides a fundamental guide for the design of ultrafast photonics based on metals.

2. Non-thermalized electron dynamics model and experimental method

2.1 Non-thermalized electron dynamics model

Gold, silver, and aluminum with similar band structures are common metals used in photonics, among which gold is usually preferred due to its chemical inertia and is used as the representative modeling system in this work. The conduction band electrons around E_F can be well described by an isotropic free-electron model. For non-thermalized electrons, the definition of electron temperature becomes invalid. Therefore, theoretical models based on temperature, such as the TTM, are not suitable to investigate non-thermalized electron dynamics. In this work, non-thermalized electron dynamics is simulated by the electron BTE as following [25, 27, 29]

$$\frac{\partial f(t,E)}{\partial t} = \left(\frac{\partial f(t,E)}{\partial t}\right)_{e-e} + \left(\frac{\partial f(t,E)}{\partial t}\right)_{e-ph} + \Phi(t,E). \quad (1)$$

Here, $f(t, E)$ is the electron energy distribution function, indicating the occupancy of electrons on energy level E at moment t. The first and the second terms on the right-hand side denote contributions from *e-e* scattering and *e-ph* scattering, respectively. The last term represents the external source, which is the excitation from the femtosecond laser.

The *e-e* scattering term can be quantified by the following equation: [25]

$$\begin{aligned}\left.\frac{df(E)}{dt}\right|_{e-e} = {} & \frac{me^4}{32\pi^3\hbar^3(\varepsilon_0\varepsilon_b)^2E_s\sqrt{E}}\iint dE_1dE_2 \\ & \times\left[\frac{\sqrt{\tilde{E}}}{\tilde{E}+E_s}+\frac{1}{\sqrt{E_s}}arctan\sqrt{\frac{\tilde{E}}{E_s}}\right]_{\tilde{E}_{\min}}^{\tilde{E}_{\max}} \\ & \times\{[1-f(E)][1-f(E_1)]f(E_2)f(E_3) \\ & -f(E)f(E_1)[1-f(E_2)][1-f(E_3)]\}. \quad (2)\end{aligned}$$

Eq. (2) is used to calculate the occupancy change induced by four-electron scattering. m is the electron mass. $E_s = \frac{(\hbar\beta q_{TF})^2}{2m}$, is the electron screening energy. q_{TF} is the Thomas-Fermi wave vector. β is determined by fitting our experimental data, fixed as 0.6 in this study. The upper and the lower limits are determined by the vector addition of the electron wave vectors in the four-electron scattering, which are given by Eq. (3):

$$\begin{aligned}\tilde{E}_{\max} &= max\left\{\left(\sqrt{E_1}+\sqrt{E_3}\right)^2;\left(\sqrt{E}+\sqrt{E_2}\right)^2\right\} \\ \tilde{E}_{\min} &= min\left\{\left(\sqrt{E_1}-\sqrt{E_3}\right)^2;\left(\sqrt{E}-\sqrt{E_2}\right)^2\right\}. \quad (3)\end{aligned}$$

The *e-ph* scattering term can be evaluated by the following equation [20]:

$$\begin{aligned}\left.\frac{df(E)}{dt}\right|_{e-ph} = {} & \frac{\Xi^2\sqrt{m}}{4\pi\rho\sqrt{2E}}\int_0^{q_D}dq\,\frac{q^3}{E_q}\{[1 \\ & -f(E)]\left[f\left(E-E_q\right)n_q\right. \\ & \left.+f\left(E+E_q\right)\left(1+n_q\right)\right] \\ & -f(E)\{\left[1-f\left(E-E_q\right)\right]\left(1+n_q\right)+\left[1-f\left(E+E_q\right)\right]n_q\}\}. \quad (4)\end{aligned}$$

In Eq. (4), Ξ is the effective deformation potential constant, which is determined as 2 eV by fitting the experimental data in this work. ρ is the gold density. q_D is the Debye wave vector of gold. n_q is the occupancy number of phonons with energy E_q. The source term can be calculated by Eq. (5).

$$\begin{aligned}\Phi(t,E) = {} & \frac{I_{abs}(t)}{(h\upsilon)^2D(E_F)}\left[f(t,E-h\upsilon)\left(1-f(t,E)\right)-\right. \\ & \left.f(t,E)\left(1-f(t,E+h\upsilon)\right)\right]. \quad (5)\end{aligned}$$

Here, $f(t, E\text{-}h\upsilon)$, $f(t, E)$, and $f(t, E+h\upsilon)$ are the occupancies of electrons on $E\text{-}h\upsilon$, E, and $E+h\upsilon$ energy levels at moment t. In our calculation, the occupancies are updated for each time step. Besides, $h\upsilon$ is the excitation photon energy. $D(E_F)$ is the density of states at the Fermi energy. $I_{abs}(t)$ calculated by Eq. (6) describes the absorbed intensity at moment t.

$$I_{abs}(t) = \frac{0.94(1-R)\cdot J}{t_p}\cdot exp\left[-2.77\left(\frac{t}{t_p}\right)^2\right]. \quad (6)$$

In Eq. (6), R is the reflectivity, J is the pump fluence, and t_p is the pump pulse width. The derivation details about the non-thermalized electron dynamics model can be found in Refs. [25], [27], and [29].

2.2 Femtosecond spectroscopy

In this work, the optical response signals for different probe photon energies are measured by femtosecond spectroscopy to characterize non-thermalized electron dynamics. The reflectance change of gold is measured in our experiment. A schematic of the experiment system is presented in Fig. 2 (a). The femtosecond laser is generated by an Yb: KGW laser (Pharos-10 W, Light Conversion) with center photon energy at 1.21 eV (1030 nm). The repetition rate of the laser is 50 kHz. The output is split into a pump beam and a probe beam through a beamsplitter. The pump photon energy is tuned to 1.48 eV (840 nm) by an optical parameter amplifier (OPA-1, Orpheus-N-2H, Light Conversion) to avoid interband transitions, which will change free electron density and E_F. The pump is modulated by a mechanical chopper at a frequency of 500 Hz. The probe photon energy is tuned through another optical parameter amplifier (OPA-2, Orpheus-F, Light Conversion). The probe light path is varied by a motorized delay stage, so that the time delay between the pump and the probe arriving at the sample can be adjusted. Then, the reflectance change at different moments after the pump excitation can be measured. A balanced detector is applied to facilitate the extraction of the weak signal. The probe is split into two arms before it arrives at the sample. One arm, as the reference light, goes into the balanced detector directly. The other one strikes the sample, and the reflected light goes into the balanced detector. The signal of reflectance change, quantified by the difference between the reflected probe and the reference, is extracted by a lock-in amplifier with the reference frequency also at 500 Hz, *i.e.* the chopping frequency. The pump and the probe are set in a non-collinear scheme to diminish the influence of the scattered pump on the signal. The gold film with thickness of 100 nm is coated on a silicon substrate by electron beam evaporation. In our experiment, the excitation power is 10 mW, the pump fluence is 14.1 J/m^2, and the full width at half

maximum of the pump pulse is 121.1 fs measured by an autocorrelator (GECO, Light Conversion).

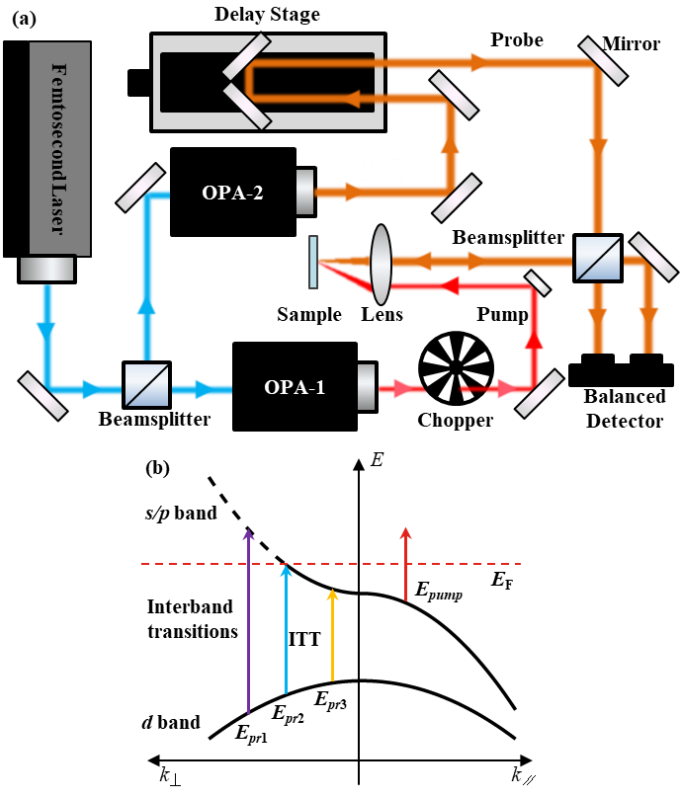

Fig. 2 (a) Schematic of the femtosecond spectroscopy system; (b) landscape of optical transitions in gold. The purple arrow means that a *d* band electron absorbs a photon with energy larger than the ITT and transitions to an energy level above E_F. The yellow arrow represents that a *d* band electron absorbs a photon with energy smaller than the ITT, and transitions to an energy level below E_F. The blue arrow corresponds to a transition from the *d* band to E_F.

The landscape of optical transitions in gold is illustrated in Fig. 2 (b). The electron energy distribution near E_F is severely changed due to the pump excitation by intraband transitions within the *s*/*p* band. The probe photon, with energy (1.91 eV - 2.7 eV) near the ITT of gold (2.47 eV), can be absorbed by interband transitions due to electron vacancy created by the pump. In Fig. 2 (b), the purple arrow means that a *d* band electron absorbs a photon with energy larger than the ITT and transitions to an energy level above E_F. The yellow arrow represents that a *d* band electron absorbs a photon with energy smaller than the ITT, and transitions to an energy level below E_F. The blue arrow corresponds to a transition from the *d* band to E_F. The evolutions of optical response for probe with different photon energies are closely related to the dynamics of electrons on different energy levels.

Revealing the physical origin of the sub-picosecond optical response requires accurate measurement of time delay in femtosecond spectroscopy, which can be realized by non-degenerate two-photon absorption experiment based on 6H-SiC (Note: in most cases, the absolute time delay is not necessary in femtosecond spectroscopy since only the relative timescale and the signal change rate are concerned). The wide bandgap of 6H-SiC (2.9 eV) is larger than the probe photon energy in this work, which prevents the one-photon absorption process. But with a pump photon, the probe photon can be absorbed due to non-degenerate two-photon absorption, as illustrated in Fig. 3 (a). The absolute temporal zero point was defined as the moment when the pump and the probe pulses arrive at the sample simultaneously. The probe relative transmission change $\Delta T/T$ varies with the time delay between the pump and the probe. As shown in Fig. 3 (b), $\Delta T/T$ is featured by a Gaussian distribution in the time domain due to the pump pulse shape. At t_3 moment (Fig. 3 (b)), the intensity peak of the pump overlaps that of the probe, and the absorption

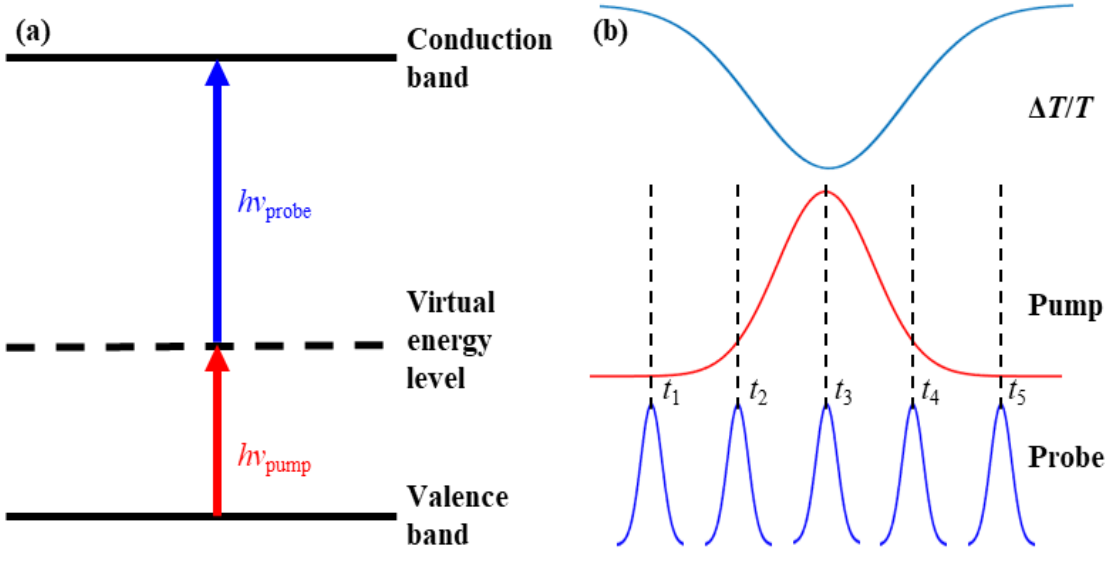

Fig. 3 (a) Illustration of non-degenerate two-photon absorption. The electron in the valence band first absorbs a pump photon and transitions to a virtual energy level. Then, it absorbs a probe photon and transitions to the conduction band. (b) Schematic of the crossing of the pump and the probe and the relative transmission change in the time domain.

cross section of the probe is maximized, leading to a valley in transmission featuring the absolute temporal zero. Hence, this transient transmission change of 6H-SiC was used to precisely calibrate the time delay. Since the crystal angle and the light path length vary with the probe photon energy in OPA-2, the temporal zero points for all probe photon energies are measured in our experiment.

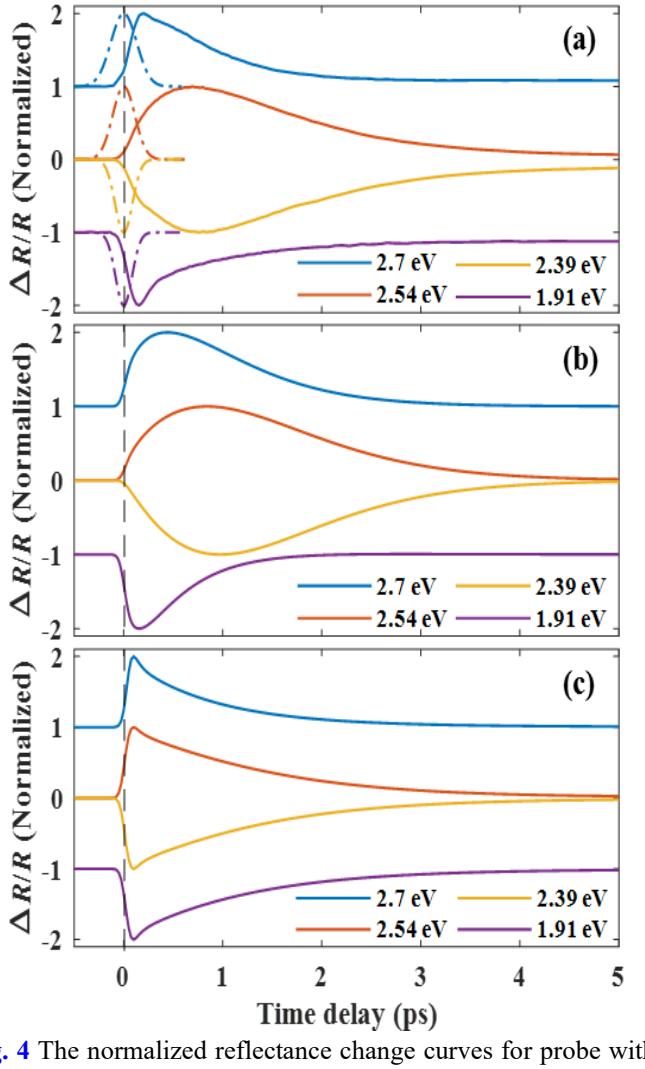

Fig. 4 The normalized reflectance change curves for probe with photon energy at 2.7 eV, 2.54 eV, 2.39 eV, and 1.91 eV: (a) experimental results (The dot-dash lines are the transmission change curves of the 6H-SiC induced by non-degenerate two-photon absorption); (b) calculated results by solving the electron BTE; (c) calculated results by solving the TTM.

3. Results and discussion

In order to uncover the physical nature causing the transient optical response, the reflectance change is calculated based on the electron energy distribution as an input, which is predicted by the electron BTE. Briefly, combining electron energy distribution with the interband and intraband transitions, the dielectric function can be obtained, and then, we can get the calculated reflectance. The details about the theoretical relationship between electron energy distribution and reflectance change can be found in our previous work.[30] Fig. 4 shows the experimental and the calculated results of the normalized reflectance change curves for probe with photon energies 2.7 eV, 2.54 eV, 2.39 eV, and 1.91 eV. The calculated results of the electron BTE and the TTM are both presented for comparison. The parameters used in the calculations are as following: the reflectivity is fixed as 0.97 for the pump,[31] the penetration depth is 12.44 nm for the pump [31], and the ballistic range is set as 100 nm in the TTM.[6] The other parameters of the TTM can be found in Ref. [32]. In Fig. 4 (a), the dot-dash lines are the transmission change curves of 6H-SiC induced by non-degenerate two-photon absorption, which are used to obtain accurate time delay. The transmission changes should be negative, but they are presented intentionally as positive to be consistent with the signal sign for probe photon energies 2.7 eV and 2.54 eV for convenience.

Comparing Figs. 4 (a), (b), and (c), the calculated results by solving the electron BTE agree better with the experimental results. The deviation for the probe photon energy 2.7 eV (the blue curve) may be because there are some other allowable transitions for this relatively high photon energy, which may also lead to a negative signal component.[25] Both the experimental and the calculated results by the electron BTE show that the leading and the tailing durations for probe photon energies 1.91 eV and 2.7 eV are obviously shorter than the durations for the other probe photon energies. This is because *e-e* scattering and *e-ph* scattering have different effects on the electrons at different energy levels. Qualitatively speaking, the larger energy difference between the electron energy and E_F, namely (E - E_F), the faster the electron dynamics induced by scattering. The optical response for probe photon energy far away from the ITT (2.47 eV) is determined by the dynamics of electrons far away from E_F. Therefore, short leading and tailing durations are measured for probe photon energy at 1.91 eV. This is consistent with the conclusion of Fermi liquid theory.[33] It is found that there is a little deviation in 0-2 ps between the experimental and simulation results in Fig. 4 (a) and Fig. 4 (b), respectively. This discrepancy can be explained by the spatial diffusion of non-thermalized electrons, which is not included in our simulation. The spatial diffusion may result in an inflection on the signal curve when the film thickness is large as indicated by the experimental results in Ref. [34]. Around 5 ps, the calculated signals are closer to zero than the experimental results for all the curves. This may be because of the following two aspects. One is that the band structure changes with heating of the lattice after excitation, while it is fixed in the simulation. The other one is that thermal strain generated by the pump heating, which is neglected in the calculation model, affects the experimental optical response.[35] The optical response signal in sub-picosecond timescale is discussed in the following in terms of non-thermalized electron dynamics. The results based on the TTM apparently fail to predict the variation of the leading and the tailing times with probe photon energy since it neglects the electron thermalization process, which will be discussed later.

Fig.5 (a) illustrates the evolution of the electron energy distribution after the sample is excited by the pump with photon energy at 1.48 eV. The color represents the electron occupancy change $\Delta f(E) = f(E) - f_0(E)$. Here, f_0 is the Fermi-Dirac distribution at 300 K. At the beginning, an obvious occupancy change can be observed in a large energy range (~ ±1 eV), which indicates a significant population of non-thermalized electrons. As time goes on, this energy range gradually narrows down to hundreds to tens of meV (~ $k_B T_e$), due to the thermalization process driven by *e-e* scattering. Fig. 5 (b) shows the electron occupancy change curves at 0 fs, 300 fs, 1 ps, and 3 ps, and the dash line represents E_F. The horizontal coordinate is divided into eight zones by the energy difference with respect to E_F, and these zones are marked as E_1, E_1', E_2, E_2', E_3, E_3', E_4, and E_4' which are filled in red, yellow, blue, and white correspondingly. When t = 0 fs, the electron occupancies are changed by the pump excitation for the electrons in E_1, E_1', E_2, E_2', E_3 and E_3' zones. When t = 300 fs, due to *e-e* scattering, the occupancy changes decrease for electrons in E_3 and E_3' zones, whereas they increase for electrons in E_1, E_1', E_2, and E_2' zones (Here, only the amplitude of the electron occupancy change and the reflectance change is considered). Around t = 1 ps, the occupancy change reaches the maximum in E_1 and E_1' zones. At this moment, the thermalization of electrons is finished. After that, dominated by *e-ph* scattering, energy transfers from electrons to phonons, and the electron occupancy changes decrease for all the electrons from t = 1 ps to t = 3 ps.

The evolution of the electron occupancy changes with energy difference from E_F by 0.23 eV, 0.07 eV, -0.08 eV and -0.56 eV is given in Fig. 6 (a). The horizontal coordinate is the time delay relative to the time when the pump arrives at the sample. The evolution is divided into three distinct stages, marked as t_1, t_2, and t_3, which are dominated by the excitation of the pump, *e-e* scattering, and *e-ph* scattering respectively. For E - E_F = 0.07 and -0.08 eV, the electron energy levels are closer to E_F. Therefore, both the pump excitation and *e-e* scattering promote the occupancy change and the leading time includes two parts, namely t_1 and t_2 stages. The decrease of the occupancy change within t_3 is dominated by *e-ph* coupling, which is a slower dynamic process compared with *e-e* scattering. For E - E_F = -0.56 eV, the electron energy level is farther away from E_F. Only the pump excitation causes the increase of the occupancy change, after which *e-e* scattering causes the occupancy change to decrease rapidly to a low level. Then *e-ph* coupling makes the residual occupancy change decrease further. Therefore, the leading time only includes t_1 stage and the tailing time includes t_2 and t_3 stages. For E - E_F = 0.23 eV, the energy difference is intermediate and thus the maximum of the occupancy falls in t_2. Intermediate leading and tailing durations are obtained for electrons on such energy level. The relative reflectance change of probe with different photon energies, which are determined by the dynamics of electrons at different energy levels, are presented in Fig. 6 (b). According to the analysis of the electron dynamics, the optical response for probe with photon energy far away from the ITT has short leading and tailing times. While both the leading and the tailing times are longer for probe with photon energy closer to the ITT. The differences in the sub-picosecond optical responses originate from the different dynamics of electron occupancy during thermalization of electrons.

Additionally, the tailing of the optical signal is also a key concern in the investigation of thermal properties, such as *e-ph* coupling strength, interface thermal conductance, and so on. Hopkins *et al.* proposed to add a time constant into the pump pulse width to get a better fitting results in the measurement of *e-ph* coupling factor. However, one time constant is only valid for a specific probe photon energy and cannot be suitable for different probe photon energies.[36] Guo and Xu mentioned that the tailing signal for probe photon energy close to the ITT

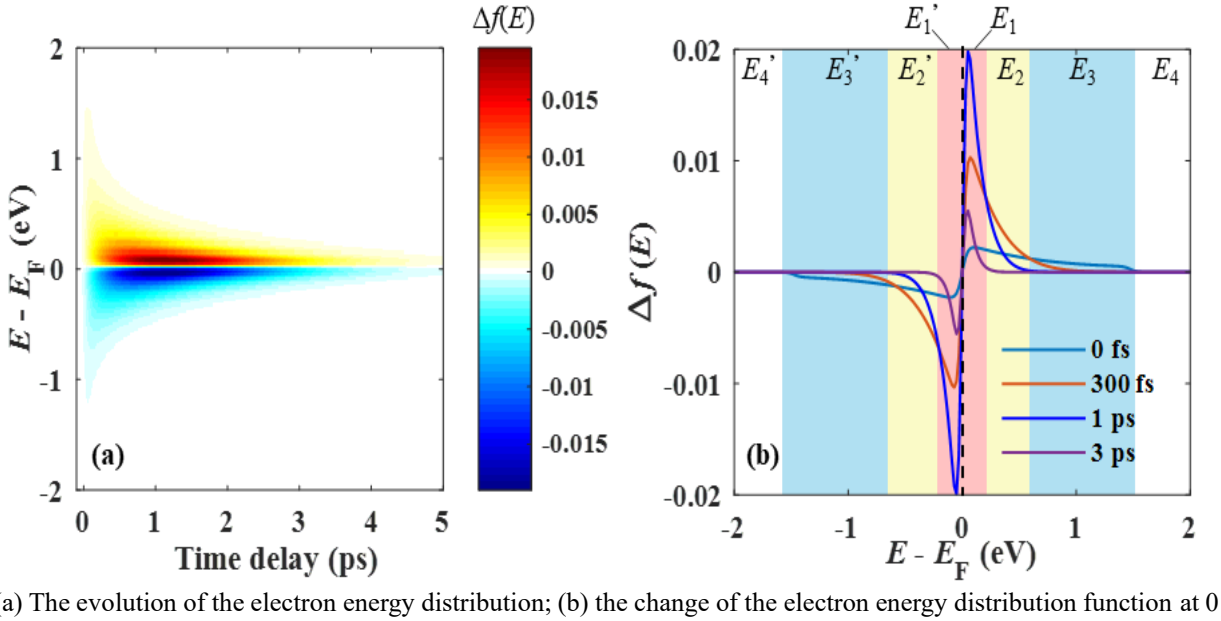

Fig. 5 (a) The evolution of the electron energy distribution; (b) the change of the electron energy distribution function at 0 fs, 300 fs, 1 ps, and 3 ps after the sample is excited by the pump with photon energy at 1.48 eV.

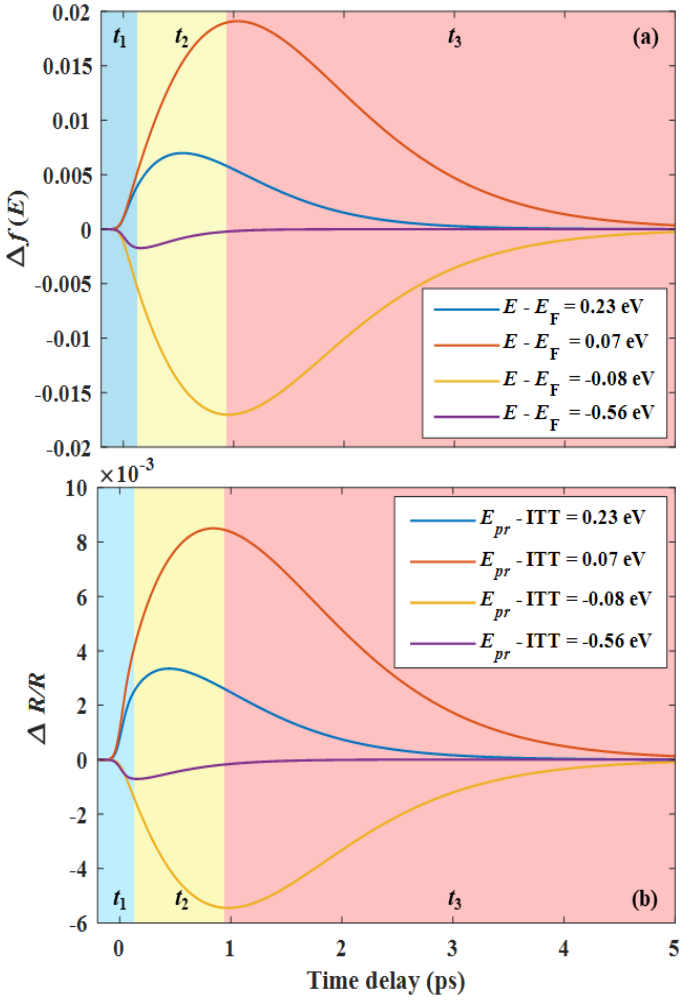

Fig. 6 (a) The theoretical energy distribution evolution of electrons with energy difference from E_F by 0.23 eV, 0.07 eV, -0.08 eV and -0.56 eV; (b) the theoretical evolution of the reflectance change of probe with energy differences from the ITT by 0.23 eV, 0.07 eV, -0.08 eV and -0.56 eV.

should be adopted to extract an accurate *e-ph* coupling factor.[37] But in that work, comparing the calculated results with the experimental results, there was always a deviation around the peak, *i.e.*, a sharper peak in calculation versus a flatter peak in experiment as shown in Fig. 4 (c). Because in their numerical model, the TTM, the electrons were assumed to be instantaneously thermalized, which cannot reflect the real thermalization process.[37] An inaccurate *e-ph* coupling strength resulting from the inappropriate selection of probe photon energy would cause an error in the study of interface heat transfer, as discussed in Ref. [37]. Besides, as seen in Fig. 4 (c), the tailing edges of the results by solving the TTM are almost the same for all the probe photon energies since *e-ph* heat transfer serves as the only origin of the decrease of the signal. However, the experimental results clearly show that the evolution of the reflectance change is closely related to the probe photon energy, as presented in Fig. 4 (a). This relationship can be well reflected by solving the electron BTE, as shown in Fig. 4 (b). An accurate coupling factor can be acquired if the probe photon energy is close to the ITT, for which the decrease of the signal is only determined by the *e-ph* heat transfer.

4. Summary

The sub-picosecond optical response of gold is investigated from the perspective of non-thermalized electron dynamics in this work. The optical responses under different probe photon energies are analyzed by the model of non-thermalized electron dynamics based on the electron BTE and femtosecond spectroscopy. For the probe with photon energy close to the ITT, the optical response of the tailing edge is slower due to the coupling between thermalized electrons and phonons. Therefore, this optical response can be used to extract the *e-ph* coupling factor, which affects the material thermal transport properties. For instance, it is demonstrated that a weak *e-ph* coupling strength results in a significant suppression of heat transfer near the interface.[38] Despite the small amplitude of the optical response signal, short leading time following the excitation pulse width and short tailing time attributed to electron thermalization are detected for the probe with photon energy far away from the ITT. With improvement by constructing photonic structures, the fast optical response with off-ITT probe can be utilized to achieve ultrafast modulation. In conclusion, the fundamental of the sub-picosecond optical response of metals due to non-thermalized electron dynamics is revealed, which provides guidance for the design of ultrafast photonic devices based on metals.

Acknowledgements

This work was supported by the National Natural Science Foundation of China (51806094 and 51776038), Characteristic Innovation Project of the Department of Education of Guangdong Province (2018KTSCX202), Centers for Mechanical Engineering Research and Education at MIT and SUSTech (Y01346002), and Center for Computational Science and Engineering of Southern University of Science and Technology.

Supporting information

Not applicable

Conflict of interest

There are no conflicts to declare.

Reference

[1] D. G. Cahill,W. K. Ford, K. E. Goodson, G. D. Mahan, A. Majumdar, H. J. Maris, R. Merlin, S. R. Phillpot, *J. Appl. Phys.*, 2003, **93**, 793-818, doi: 10.1063/1.1524305.

[2] D. G. Cahill, P. V. Braun, G. Chen, D. R. Clarke, S. Fan, K. E. Goodson, P. Keblinski, W. P. King, G. D. Mahan, A. Majumdar, H. J. Maris, S. R. Phillpot, E. Pop, L. Shi, *Appl. Phys. Rev.*, 2014, **1**,011305, doi: 10.1063/1.4832615.

[3] L. Qiu, N. Zhu, H. Zou, Y. Feng, X. Zhang, D. Tang, *Int. J. Heat Mass Tran.*, 2018, **125**, 413-433, doi: 10.1016/j.ijheatmasstransfer.2018.04.087.

[4] Z. Lu, X. Ruan, *ES Energy Environ.*, 2019, **4**, 5-14, doi: 10.30919/esee8c155.
[5] T. Q. Qiu, T. Juhasz, C. Suarez, W. E. Bron, C. L. Tien, *Int. J. Heat Mass Tran.*, 1994, **37**, 2799-2808, doi: 10.1016/0017-9310(94)90397-2.
[6] J. Hohlfeld, S. S. Wellershoff, J. Güdde, U. Conrad, V. Jähnke, E. Matthias, *Chem. Phys.*, 2000, **251**, 237-258. doi: 10.1016/S0301-0104(99)00330-4.
[7] W. G. Ma, H. D. Wang, X. Zhang, W. Wang, *J. App. Phys.*, 2010, **108**, 064308, doi:10.1063/1.3482006.
[8] H. Bao, J, Chen, X. Gu, B. Cao, *ES Energy Environ.*, 2018, **1**, 16-55, doi:10.30919/esee8c149.
[9] A. Giri, B. M. Foley, P. E. Hopkins, *J. Heat Trans-T ASME*, 2014, **136**, 092401, doi:10.1115/1.4027785.
[10] Z. Lu, Y. Wang, X. Ruan, *Phys. Rev. B*, 2016, **93**, 064302, doi: 10.1103/PhysRevB.93.064302.
[11] L. Qiu, H. Zou, X. Wang, Y. Feng, X. Zhang, J. Zhao, X. Zhang, Q. Li, *Carbon*, 2019, **141**, 497-505, doi: 10.1016/j.carbon.2018.09.073.
[12] Y. Wang, Z. Lu, A. K. Roy, X. Ruan, *J. Appl. Phys.*, 2016, **119**, 065103, doi: 10.1063/1.4941347.
[13] A. Giri, J. T. Gaskins, B. F. Donovan, C. Szwejkowski, R. J. Warzoha, M. A. Rodriguez, J. Ihlefeld, P. E. Hopkins, *J. Appl. Phys.*, 2015, **117**, 105105, doi: 10.1063/1.4914867.
[14] Z. Lu, A. Vallabhaneni, B. Cao, X. Ruan, *Phys. Rev.* B, 2018, **98**, 134309, doi: 10.1103/PhysRevB.98.134309.
[15] S. Xu, A. Fan, H. Wang, X. Zhang, X. Wang, *Int. J. Heat Mass Tran.*, 2020, **154**, 119751, doi: 10.1016/j.ijheatmasstransfer.2020.119751.
[16] K. C. Phillips, H. H. Gandhi, E. Mazur, S. K. Sundaram, *Adv. Opt. Photonics*, 2015, **7**, 684-712, doi: 10.1364/AOP.7.000684.
[17] L. Jiang, A. D. Wang, B. Li, T. H. Cui, Y. F. Lu, *Light-Sci. Appl.*, 2018, **7**, 17134, doi: 10.1038/lsa.2017.134.
[18] Z. Chai, X. Hu, F. Wang, X. Niu, J. Xie, Q. Gong, *Adv. Optical Mater.*, 2017, **5**, 1600665, doi: 10.1002/adom.201600665.
[19] M. Taghinejad, W. Cai, *ACS Photonics*, 2019, **6**, 1082–1093, doi: 10.1021/acsphotonics.9b00013.
[20] G. Grinblat, R. Berté, M. P. Nielsen, Y. Li, R. F. Oulton, S. A. Maier, *Nano Lett.*, 2018, **18**, 7896-7900, doi: 10.1021/acs.nanolett.8b03770.
[21] L. H. Nicholls, T. Stefaniuk, M. E. Nasir, F. J. Rodriguezfortuno, G. A. Wurtz, A. V. Zayats, *Nat. Commun.*, 2019, **10**, 2967, doi: 10.1038/s41467-019-10840-7.
[22] M. Taghinejad, H. Taghinejad, Z. Xu, Y. Liu, S. P. Rodrigues, K. Lee, T. Lian, A. Adibi, W. Cai, *Adv. Mater.*, 2018, **30**, 1704915, doi: 10.1002/adma.201704915.
[23] M. Taghinejad, H. Taghinejad, Z. Xu, K. Lee, S. P. Rodrigues, J. Yan, A. Adibi, T. Lian, W. Cai, *Nano Lett.*, 2018, **18**, 5544-5551, doi: 10.1021/acs.nanolett.8b01946.
[24] C. Sun, F. Vallee, L. H. Acioli, E. P. Ippen, J. G. Fujimoto, *Phys. Rev. B*, 1994, **50**, 15337-15348, doi: 10.1103/PhysRevB.50.15337.
[25] N. D. Fatti, C. Voisin, M. Achermann, S. Tzortzakis, D. Christofilos, F. Vallee, *Phys. Rev. B*, 2000, **61**, 16956-16966, doi: 10.1103/PhysRevB.61.16956.
[26] M. Lisowski, P. A. Loukakos, U. Bovensiepen, J. Stähler, C. Gahl, M. Wolf, *Appl. Phys. A*, 2004,**78**, 165-176, doi: 10.1007/s00339-003-2301-7.
[27] L. D. Pietanza, G. Colonna, S. Longo, M. Capitelli, *Eur. Phys. J. D*, 2007, **45**, 369-389, doi: 10.1140/epjd/e2007-00251-1.
[28] T. Heilpern, M. Manjare, A. O. Govorov, G. P. Wiederrecht, S. K. Gray, H. Harutyunyan, *Nat. Commun.*, 2018, **9**, 1-6, doi: 10.1038/s41467-018-04289-3.
[29] S. Longo, L. D. Pietanza, F. A. Tassielli, M. Capitelli, *Laser Part. Beams*, 2002, **20**, 285, doi: 10.1017/S0263034602202190.
[30] L. Zhang, W. Li, L. Zhang, Y. Zhong, X. Guo, L. Li, E. N. Wang, L. Guo, *J. Appl. Phys.*, 2020, **128**, 055107, doi: 10.1063/5.0015586.
[31] B. H. Billings, D. E. Gray, American Institute of Physics Handbook, McGraw-Hill, 1972. ISBN: 007001485X.
[32] I. H. Chowdhury, X. Xu, *Numer. Heat Trans. A: Appl.*, 2003, **44**, 219-232, doi: 10.1080/716100504.
[33] N. W. Ashcroft, N. Mermin, Solid State Physics, Cornell University, 1976. ISBN: 0030839939.
[34] L. Guo, S. L. Hodson, T. S. Fisher, X. Xu, *J. Heat Trans-T ASME.*, 2012, **134**, 042402, doi: 10.1115/1.4005255.
[35] W. Ma, T. Miao, X. Zhang, M. Kohno, Y. Takata, *J. Phys. Chem. C*, 2015, **119**, 5152-5159, doi: 10.1021/jp512735k.
[36] P. E. Hopkins, L. M. Phinney, J. R. Serrano, *J. Heat Trans-T ASME.*, 2011, **133**, 044505, doi: 10.1115/1.4002778.
[37] L. Guo, X. Xu, *J. Heat Trans -T ASME*, 2014, **136**, 122401, doi: 10.1115/1.4028543.
[38] R. B. Wilson, J. P. Feser, G. T. Hohensee, D. G. Cahill, *Phys. Rev. B*, 2013, **88**, 144305, doi: 10.1103/PhysRevB.88.144305.

Author information

***Long Li**, a joint post-doctor of Southern University of Science and Technology and Southeast University. The main research direction is ultrafast laser-material interaction.*

***Zhen Chen**, a professor in School of Mechanical Engineering, Southeast University in China. His research direction includes the transport, storage, and conversion of the basic carriers in nanoscale.*

***Liang Guo**, an assistance professor in Department of Mechanical and Energy Engineering, Southern University of Science and Technology in China. He is interested in the interaction between ultrafast laser and materials.*